Radiology

Psychoradiologic Utility of MR Imaging for Diagnosis of Attention Deficit Hyperactivity Disorder: A Radiomics Analysis[1]

Huaiqiang Sun, PhD
Ying Chen, MD, PhD
Qiang Huang, PhD
Su Lui, PhD
Xiaoqi Huang, PhD
Yan Shi, MD
Xin Xu, MD
John A. Sweeney, PhD[2]
Qiyong Gong, MD, PhD

Purpose: To identify cerebral radiomic features related to diagnosis and subtyping of attention deficit hyperactivity disorder (ADHD) and to build and evaluate classification models for ADHD diagnosis and subtyping on the basis of the identified features.

Materials and Methods: A consecutive cohort of 83 age- and sex-matched children with newly diagnosed and never-treated ADHD (mean age 10.83 years ± 2.30; range, 7–14 years; 71 boys, 40 with ADHD-inattentive [ADHD-I] and 43 with ADHD-combined [ADHD-C, or inattentive and hyperactive]) and 87 healthy control subjects (mean age, 11.21 years ± 2.51; range, 7–15 years; 72 boys) underwent anatomic and diffusion-tensor magnetic resonance (MR) imaging. Features representing the shape properties of gray matter and diffusion properties of white matter were extracted for each participant. The initial feature set was input into an all-relevant feature selection procedure within cross-validation loops to identify features with significant discriminative power for diagnosis and subtyping. Random forest classifiers were constructed and evaluated on the basis of identified features.

Results: No overall difference was found between children with ADHD and control subjects in total brain volume (1 069 830.00 mm^3 ± 90 743.36 vs 1 079 213.00 mm^3 ± 92 742.25, respectively; P = .51) or total gray and white matter volume (611 978.10 mm^3 ± 51 622.81 vs 616 960.20 mm^3 ± 51 872.93, respectively; P = .53; 413 532.00 mm^3 ± 41 114.33 vs 418 173.60 mm^3 ± 42 395.48, respectively; P = .47). The mean classification accuracy achieved with classifiers to discriminate patients with ADHD from control subjects was 73.7%. Alteration in cortical shape in the left temporal lobe, bilateral cuneus, and regions around the left central sulcus contributed significantly to group discrimination. The mean classification accuracy with classifiers to discriminate ADHD-I from ADHD-C was 80.1%, with significant discriminating features located in the default mode network and insular cortex.

Conclusion: The results of this study provide preliminary evidence that cerebral morphometric alterations can allow discrimination between patients with ADHD and control subjects and also between the most common ADHD subtypes. By identifying features relevant for diagnosis and subtyping, these findings may advance the understanding of neurodevelopmental alterations related to ADHD.

Online supplemental material is available for this article.

[1] From the Department of Radiology, Huaxi MR Research Center (H.S., Y.C., S.L., X.H., J.A.S., Q.G.), Research Core Facilities (H.S., Q.H.), and Department of Psychiatry (Y.C., Y.S., X.X.), West China Hospital of Sichuan University, Chengdu, Sichuan 610041, China; Department of Psychoradiology, Chengdu Mental Health Center, Chengdu, Sichuan, China (Y.C., Y.S., X.X., Q.G.); and Department of Psychology, School of Public Administration, Sichuan University, Chengdu, Sichuan, China (Y.S.,Q.G.). Received February 3, 2017; revision requested April 17; revision received June 18; accepted July 14; final version accepted August 24. **Address correspondence to** Q.G. (e-mail: *qiyonggong@hmrrc.org.cn*).

Study supported by the National Natural Science Foundation of China (81030027, 81220108013, 81227002, 81601458, 81621003), the Ministry of Education of the People's Republic of China (IRT16R52), and the Ministry of Science and Technology of the People's Republic of China (2016YFC0100803). Q.G. supported by Changjiang Scholar Professorship Award (T2014190) of China and American CMB Distinguished Professorship Award (F510000/G16916411) administered by the Institute of International Education, USA.

Current address:
[2] Department of Psychiatry and Behavioral Neuroscience, University of Cincinnati, Cincinnati, Ohio.

H.S. and Y.C. contributed equally to this work.

Attention deficit hyperactivity disorder (ADHD), characterized by age-inappropriate inattention, hyperactivity, and impulsivity, is among the most common childhood-onset neurodevelopmental disorders, with an estimated prevalence in 5%–8% of children and 4% of adults worldwide (1). ADHD has an adverse effect on social, cognitive, educational, and emotional functions (2–6). Currently, clinical diagnosis and subtyping of ADHD is based on an integration of parent and teacher behavioral reports and assessment of behavioral problems (7). However, given the subjective nature of these evaluations and the overlap of ADHD with other psychiatric disorders, imaging-based parameters may provide a useful objective adjunct to clinical psychiatric evaluation for diagnosing and subtyping ADHD.

Although the etiology and neurobiological substrate of ADHD remain unclear, converging evidence from imaging studies suggests that individuals with ADHD have alterations in brain volume (8–11), cortical morphometric features (12–14), and diffusion properties of white matter tracts (15) when compared with typically developing individuals. However, previous imaging findings have no established diagnostic value for individual patients with ADHD, as studies typically report group-level differences between patients and control subjects. Analyzing brain imaging data under the framework of machine learning has the potential to address this challenge (16). In the context of the developing field of psychoradiology (17), machine learning is concerned with automatic discovery of regularities in brain imaging data through the use of pattern recognition algorithms to develop classifiers that can be used to predict disorders in individuals.

The first step in building an image-based classifier is to extract quantitative features from brain images. Voxel-wise features, which have been widely used as extracted features in previous neuroimage-based classification studies (18–20), are sensitive to registration errors and intersubject variations and present the problem of dimensionality. The emerging field of radiomics has the potential to address this problem (21). Radiomics is a medical image analysis framework that converts digital radiographic images into a mineable data set with a series of data characterization algorithms. It has been applied mainly in clinical oncology to extract imaging features in solid tumors. The first step of a radiomics workflow for oncology has been to segment tumors on medical images, after which quantitative imaging features are extracted. Extracted features represent the intensity distribution, shape, and texture of tumors and capture distinct phenotypes of tumors that are clinically important (22). Similarly, brain magnetic resonance (MR) images also can be analyzed within a radiomics framework by precisely segmenting the brain into anatomic structures and then extracting quantitative features from segmented structures to form the mineable data set.

However, radiomics features may also present the high-dimension low–sample size problem (23). Common practice in machine learning is to perform feature selection to reduce the dimensionality by selecting the features that carry useful information related to category label. However, similar to the issue of feature selection in genetics research, the features from neuroimaging data can also be highly correlated because of the intrinsic network architecture of the human brain (24,25). Thus, it is crucial to identify all the relevant features related to the disease during

Advances in Knowledge

- Cerebral radiomic features based random forest models allowed discrimination of patients with attention deficit hyperactivity disorder (ADHD) from healthy control subjects with 73.7% mean accuracy and discrimination of ADHD inattentive and combined inattentive and hyperactive subtypes with 80.1% mean accuracy in a MR imaging study with a single imager and amedication-naïve and relatively large sample size.
- During model construction, the all-relevant feature selection process identified alteration in cortical shape within the left temporal lobe, bilateral cuneus, and regions around left central sulcus that contributed significantly to group discrimination, while features involved in the default mode network and insular cortex had significant contribution to subtype discrimination.

Implications for Patient Care

- The proposed analysis framework based on radiomics and machine learning has the ability to identify imaging features relevant to diagnosing ADHD, while furthering the understanding of neurologic developmental alterations related to ADHD and their specific pattern in the two most common subtypes of the illness.
- The proposed analysis framework is fully automatic and can be deployed readily in clinical environments to be a useful adjunct to psychiatric behavioral evaluation for diagnosing ADHD.

https://doi.org/10.1148/radiol.2017170226

Content code: NR

Radiology 2018; 000:1–11

Abbreviations:

ADHD = attention deficit hyperactivity disorder
ADHD-C = ADHD combined subtype (inattentive and hyperactive)
ADHD-I = ADHD inattentive subtype

Author contributions:

Guarantors of integrity of entire study, H.S., Q.G.; study concepts/study design or data acquisition or data analysis/interpretation, all authors; manuscript drafting or manuscript revision for important intellectual content, all authors; approval of final version of submitted manuscript, all authors; agrees to ensure any questions related to the work are appropriately resolved, all authors; literature research, H.S., Q.H., S.L., Y.S., X.X., J.A.S., Q.G.; clinical studies, Y.C., S.L., X.H., Y.S., X.X., J.A.S., Q.G.; experimental studies, H.S., Q.G.; statistical analysis, H.S., Q.H., J.A.S., Q.G.; and manuscript editing, H.S., Q.H., Y.S., X.X., J.A.S., Q.G.

Conflicts of interest are listed at the end of this article.

the classification process, because understanding the mechanisms behind the imaging phenotype is the aim. Therefore, the purpose of our study was to identify all cerebral radiomics features related to ADHD diagnosis and subtyping and to build and evaluate classification models for ADHD diagnosis and subtyping on the basis of the identified features.

Materials and Methods

Participants

This prospective study was approved by the local ethics committee for human studies. All participants and their parents were fully informed about the purpose and procedures of this study, written informed consent was obtained from the parents, and assent was provided by child participants before enrollment. Study participants were consecutively recruited from September 2009 to October 2015. Children with newly diagnosed and never-treated ADHD were recruited from the Department of Psychiatry, West China Hospital, Sichuan University. Diagnosis of ADHD was determined by two experienced clinical psychiatrists (Y.C. and a nonauthor, with 5 and 28 years of experience in clinical psychiatry, respectively) by using the Chinese version of the Structured Clinical Interview for Diagnotic and Statistical Manual 4 Text Revision Axis I Disorders, or SCID. The diagnosis of ADHD inattentive subtype (ADHD-I) required seven symptoms of inattention and less than four symptoms of hyperactivity and impulsivity. For a diagnosis of ADHD combined subtype (ADHD-C), seven symptoms of inattention and seven symptoms of hyperactivity or impulsivity were required. Patients with any Axis I psychiatric comorbid disorders were excluded. Other exclusion criteria were a full-scale intelligence quotient lower than 90 based on an age-appropriate Wechsler Intelligence Scale for Children, Chinese Revision results; current or past treatment with psychotropic medication; substance abuse; left-handedness (assessed by using the Annett Hand Preference Questionnaire); any physical illness that might affect brain anatomy and function (including neurologic illness; head injury; and liver, renal or cardiac abnormalities); and contraindications to MR imaging. One hundred sixteen patients underwent MR imaging, and 33 patients were excluded for the following reasons: excessive motion artifacts or inability to remain in the imager for a repetition sequence (n = 21) and vibration artifacts in diffusion data (n = 12). Finally, 83 patients (40 with ADHD-I and 43 with ADHD-C) were included in this study.

Healthy control subjects were recruited from local schools with an advertisement and were matched with patients with the same age distribution and sex ratio. Control subjects were screened by using the Chinese modified version of SCID-I (nonpatient version) to exclude any Axis I psychiatric diagnoses. Control subjects had no history of taking psychotropic medications or known family history of psychotic or mood disorder or ADHD in a first-degree relative. Other exclusion criteria were the same as those for the ADHD group. An experienced neuroradiologist (nonauthors, with 5 years of experience in diagnostic neuroimaging) inspected conventional MR imaging examinations of all participants to exclude individuals with gross neuroradiologic abnormalities (including any neurologic or systemic illness that could confound assessment of ADHD-specific brain abnormalities such as intracranial tumor; head trauma; developmental deformity; and demyelinating, infectious, and metabolic diseases). One hundred nine healthy control subjects underwent MR imaging, 22 of whom were excluded for excessive motion artifacts or vibration artifacts. Finally, 87 healthy control subjects were included in this study.

Data Acquisition

All examinations were performed by using an MR imager (Siemens Trio 3 T; Siemens Healthineers, Erlangen, Germany). High-spatial-resolution T1-weighted and diffusion-tensor imaging data (2 × 20 diffusion-encoding directions) were acquired from each participant. Imaging protocols appear in Appendix E1 (online).

Extraction of Gray Matter Features

T1-weighted anatomic images were processed with software ("recon-all" processing pipeline; Freesurfer, *https://surfer.nmr.mgh.harvard.edu/*, with the Desikan-Killiany-Tourville atlas [26] and "antsCorticalThickness" pipeline; Advanced Normalization Tools, *http://stnava.github.io/ANTs/*) (27) to generate labeled brains (full list of regional labels in Table E1 [online]). A total of 2338 shape-related features that represent gray matter morphometry were extracted from each T1-weighted image by using open source software (Mindboggle, *http://www.mindboggle.info/*) (28). Details about gray matter feature extraction appear in Appendix E1 (online).

White Matter Features Extraction

Routine diffusion-tensor processing, including head motion and eddy-current correction, brain extraction, and tensor model fitting were performed by using software (FSL, FMRIB Software Library; *http://www.fmrib.ox.ac.uk*). The Johns Hopkins University of Medicine International Consortium of Brain Mapping diffusion-tensor imaging white matter atlas constructed with data from 81 individuals, or JHU-ICBM-DTI-81, was wrapped to individual space. Distribution metrics (mean, standard deviation, skew, and kurtosis) were extracted from diffusion parameter maps (fractional anisotropy, mean diffusivity, axial diffusivity, and radial diffusivity) for each label defined in the atlas. A total of 768 features that represent the diffusion properties of white matter regions were extracted from each participant's diffusion-tensor data. Details about white matter feature extraction appear in Appendix E1 (online). The whole feature extraction process is illustrated in Figure 1.

All-Relevant Feature Selection

The morphometric features and diffusion features were concatenated into a

Figure 1

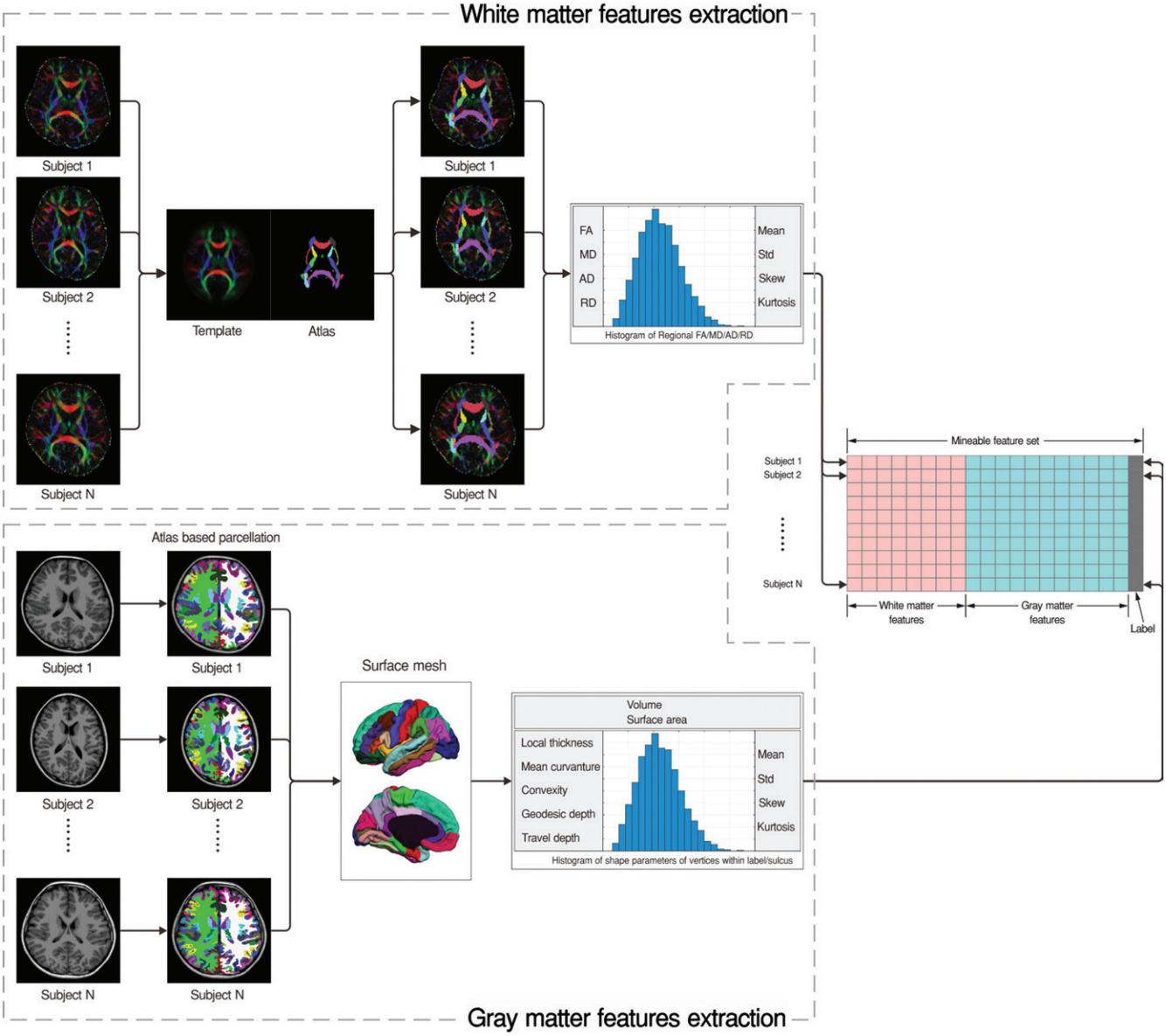

Figure 1: Diagram shows workflow for extracting radiomics features from T1-weighted and diffusion-tensor images. For extraction of gray matter features, labeled brain data were converted to surface mesh. Volume and surface area were measured for each labeled region, and shape properties (local cortical thickness, mean curvature, convexity, geodesic depth, and travel depth) were calculated on each vertex, then distribution metrics (mean, standard deviation, skew, kurtosis) of shape properties in each labeled region and sulcus were extracted. For white matter features extraction, the JHU-ICBM-DTI-81 atlas was wrapped to individual space, and istribution metrics (mean, standard deviation *[Std]*, skew, kurtosis) were extracted from four diffusion parameters: fractional anisotropy *(FA)*, mean diffusivity *(MD)*, axial diffusivity *(AD)*, and radial diffusivity *(RD)* maps for each labeled region.

long feature vector to represent both gray and white matter profiles of each individual brain (2338 morphometric and 768 diffusion features, for a total of 3106 features). To remove nonrelevant features and identify all brain regions involved in ADHD, we performed a random forest–based feature selection algorithm for all relevant features, which was implemented with software (R package, "Boruta"; *https://www.r-project.org/*) (29) on extracted features (Appendix E1 [online]). The result of the algorithm is the assignment of each feature to one of two classes: relevant or irrelevant. In our study, all relevant features were selected and compared between patients with ADHD and

Figure 2

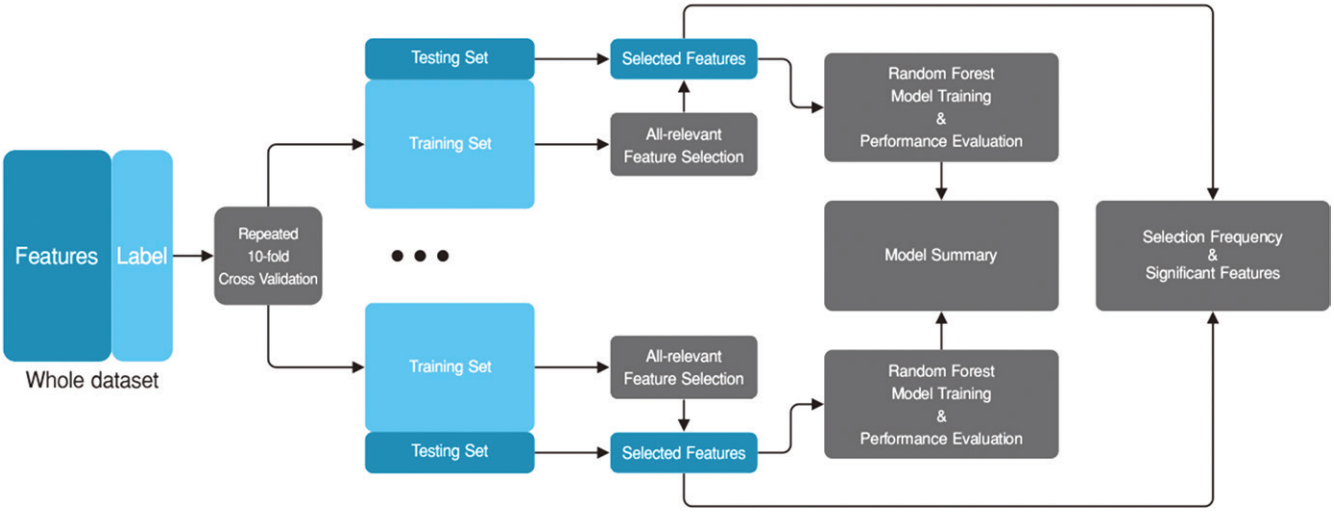

Figure 2: Flowchart shows feature selection and model training. Rectangles in blue represent data and rectangles in gray represent the processes. The all-relevant features selection step was nested in repeated 10-fold cross validation.

healthy control subjects and between ADHD subtypes.

Random Forest Classifier Training and Cross-Validation

The random forest classifier for discriminating between patients with ADHD and healthy control subjects and the classifier for discriminating between ADHD subtypes were constructed and evaluated through the workflow shown in Figure 2. The all-relevant feature selection step was embedded in a repeated *k*-fold ($k = 10$) cross-validation framework (30) to obtain unbiased estimates of classification error (31). The R package "caret" (classification and regression training) was used to implement the workflow. The overall accuracy, sensitivity, and specificity and κ score were used to characterize the performance of the classifier (Appendix E1 [online]).

Assessment of the Relevance of Selected Features

In our workflow, features were selected in each iteration on different subsets of features taken from the cross-validation procedure. Features that were selected in more iterations than would be expected to occur at random were identified as significantly relevant selections. To determine the relevance of selected features, 1000 random data sets were created by permuting the label column of the original data set. The random data sets went through the same feature selection procedure. The expected distribution of selection frequency (defined as the number of iterations in which a feature was selected divided by the total number of iterations performed in one data set) of each feature throughout cross-validation iterations was modeled as a binomial distribution with the parameter estimated as the mean selection frequency in all random data sets. This distribution was then used to find features in the original data set with selection frequency significantly higher than would be expected by chance, with adjusted *P* values of .05, after Holm-Bonferroni correction to correct for multiple tests (32).

Results

Demographic and Volumetric Comparison

Demographic variables and macroscopic cerebral volume were not significantly different between patients and control subjects or between patients with the ADHD subtypes (Tables 1, 2).

Classification Performance

In building and evaluating the classifier for discriminating patients with ADHD from healthy control subjects, we performed 100 runs of 10-fold cross-validation and summarized the classifier performance from a total of 1000 training-testing cycles. The classification accuracy and κ value achieved with our method by means of a repeated 10-fold cross-validation were 73.7% ± 5.2 and 0.47 ± 0.10, respectively, with features from the all-relevant features selection step. Sensitivity and specificity for discriminating patients with ADHD from control subjects were 70.2% ± 7.1 and 77.0% ± 5.8, respectively. In building and evaluating the classifier for discriminating between ADHD subtypes, the mean classification accuracy and κ value achieved by means of repeated 10-fold cross-validation were 80.1% ± 6.2 and 0.60 ± 0.13, respectively. Sensitivity and specificity for classifying patients with ADHD-I subtype were 71.0% ± 8.3 and 87.5% ± 5.9, respectively.

Significantly Relevant Features

As we embedded the feature selection into the cross-validation procedure, a total of 1000 feature subsets were obtained in each classifier construction.

Table 1

Demographic and Macroscopic Volume Comparison between Patients with ADHD and Healthy Control Subjects

Characteristic or Volume Measure	ADHD (n = 83)	Control Subjects (n = 87)	Statistic*	Degrees of Freedom	P Value
Age (y)	10.83 ± 2.30 (7–14)	11.21 ± 2.51 (7–15)	−1.01	168	.31
Sex†			0.12‡	1	.72
Male	71	72			
Female	12	15			
Total gray matter volume (mm^3)	611 978.10 ± 51 622.81	616 960.20 ± 51 872.93	−0.63	168	.53
Total white matter volume (mm^3)	413 532.00 ± 41 114.33	418 173.60 ± 42 395.48	−0.72	168	.47
Subcortical region volume (mm^3)	44 319.48 ± 3514.38	44 079.05 ± 3144.57	0.47	168	.64
Total brain volume (mm^3)	1 069 830.00 ± 90 743.36	1 079 213.00 ± 92 742.25	−0.67	168	.51

Note.—Unless otherwise indicated, data are means ± standard deviation, with the range in parentheses, if applicable.

* Unless otherwise indicated, statistics were calculated with *t* tests.

† Data are number of patients.

‡ χ^2 test was used.

Table 2

Demographic Characteristics and Macroscopic Volume Comparisons between Patients with ADHD-I and ADHD-C

Characteristic and Volume Measure	ADHD-I (n = 40)	ADHD-C (n = 43)	Statistic*	Degrees of Freedom	P Value
Age (y)	10.66 ± 2.23	10.91 ± 2.29	−0.48	81	.63
Sex†			0‡	1	>.99
Male	34	37			
Female	6	6			
Total gray matter volume (mm^3)	611 031.90 ± 40 442.30	611 636.90 ± 57 724.25	−0.05	81	.96
Total white matter volume (mm^3)	408 586.80 ± 36 980.55	420 132.70 ± 46 000.69	−1.19	81	.24
Subcortical region volume (mm^3)	44 022.64 ± 3232.51	44 780.13 ± 3693.04	−0.94	81	.35
Total brain volume (mm^3)	1 063 641.00 ± 75 673.49	1 076 550.00 ± 102 658.70	−0.62	81	.54

Note.—Unless otherwise indicated, data are means ± standard deviation, with the range in parentheses, if applicable.

* Unless otherwise indicated, statistics were calculated with *t* tests.

† Data are number of patients.

‡ χ^2 test was used.

In the construction of the classifier discriminating patients with ADHD from healthy control subjects, the mean number of features in each subset was 13.2 (range, eight to 17; 0.26%–0.55% of all features). Eight features were identified as significantly relevant, because their selection frequency in real data were significantly higher than that in random data (Table 3, Fig 3). In the construction of the classifier to discriminate between ADHD subtypes, the mean number of features in each subset was 8.7 (range, six to 13; 0.20%–0.42% of all features). Five significant features were identified as significantly relevant (Table 4, Fig 4).

Discussion

The major finding of this study was that cerebral radiomics-based classification models provided discrimination of patients with ADHD from healthy control subjects, as well as separation of the two most common subtypes in a medication-naïve and relatively large sample-size single-imager MR imaging study. During model construction, the all-relevant features selection process identified alteration in cortical shape in the left temporal lobe, bilateral cuneus, and regions around the left central sulcus that contributed significantly to discrimination of patients with ADHD from control subjects, while features involved in default mode network and insular cortex significantly contributed to ADHD subtype discrimination.

The aim to diagnose ADHD according to neuroimaging data has long been pursued. The largest attempt to classify ADHD by using neuroimaging data comes from the ADHD-200 consortium multicenter study in which resting-state functional and structural data sets of 285 children and adolescents with ADHD and 491 healthy control subjects were used (33). Various combinations of feature extraction and classification algorithms were used to classify this sample, with accuracy of 43.1%–61.5% (mean, 56.0%) with the use of a two-class classifier to differentiate patients with ADHD from healthy control

Table 3

Significant Features for Discriminating Patients with ADHD and Healthy Control Subjects

Selection Frequency (%)*	Hemisphere	Label or Sulcus	Feature Type†	Statistic	Patients with ADHD	Control Subjects
92.3	Left	Superior temporal sulcus	Convexity	Skew	−0.81 ± 0.11	−0.78 ± 0.08
88.4	Right	Cuneus	Local thickness	Mean	2.01 ± 0.16	1.92 ± 0.17
85.9	Left	Precentral	Mean curvature	Kurtosis	−0.33 ± 0.43	−0.41 ± 0.51
82.4	Left	Superior temporal	Travel depth	Skew	−0.46 ± 0.13	−0.40 ± 0.11
80.0	Left	Precentral	Mean curvature	Skew	−1.12 ± 0.10	−1.10 ± 0.09
77.3	Left	Cerebral peduncle	Fractional anisotropy	Skew	−0.14 ± 0.16	−0.24 ± 0.15
76.9	Left	Cuneus	Local thickness	Mean	1.89 ± 0.15	1.85 ± 0.18
75.1	Left	Postcentral	Mean curvature	Kurtosis	−0.26 ± 0.66	−0.48 ± 0.46

Note.—Unless otherwise indicated, data are means ± standard deviation.

* Defined as number of iterations in which the feature was selected divided by the total number of iterations performed.

† Includes local thickness, mean curvature, convexity, geodesic depth, and travel depth for gray matter structure and fractional anisotropy, mean diffusivity, axial diffusivity, and radial diffusivity for white matter structure.

Figure 3

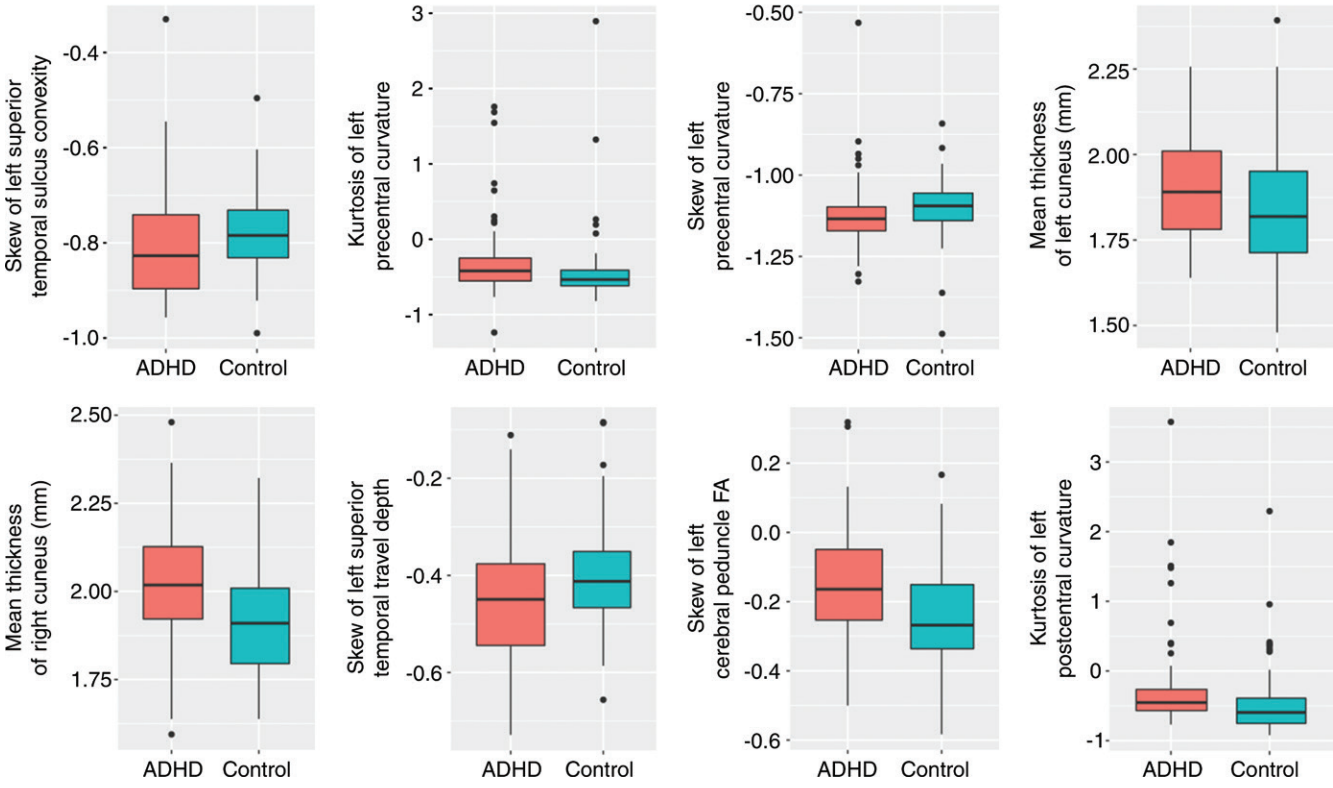

Figure 3: Graphs show distribution of significant features that discriminated ADHD and healthy control subjects. *FA* = fractional anisotropy.

subjects. The best classifier achieved high specificity of 94% but poor sensitivity of 21%, resulting in overall accuracy of 61%. One limitation to these findings was that resting-state functional MR imaging data suffers from inconsistent echo-planar imaging acquisition provided by different imaging systems and manufacturers, and these differences likely increased variability in brain measurements related to the patients' state of illness. Furthermore, the approach used involved sophisticated data preprocessing steps, which are not feasible in a clinical environment. Also, the lack of diffusion-weighted MR imaging data may have limited the efficiency of the constructed classifier, because

Table 4

Significant Features for Discriminating ADHD-I and ADHD-C Subtypes

Selection Frequency (%)*	Hemisphere	Label/Sulcus	Feature Type†	Statistics	Patients with ADHD-I	Patients with ADHD-C
93.7	Left	Circular sulcus	Travel depth	Mean	19.75 ± 1.26	20.05 ± 1.12
90.1	Left	Posterior cingulate	Mean curvature	Skew	−1.13 ± 0.08	−1.17 ± 0.11
85.4	Left	Sylvian fissure	Mean curvature	Kurtosis	−0.407 ± 0.30	−0.31 ± 0.34
82.7	Left	Pars triangularis	Mean curvature	Kurtosis	−0.85 ± 0.16	−0.72 ± 0.16
77.5	Left	External capsule	Fractional anisotropy	Skew	0.13 ± 0.14	0.20 ± 0.20

Note.—Unless otherwise indicated, data are means ± standard deviation.

* Defined as number of iterations in which the feature was selected divided by total number of iterations performed.

† Includes local thickness, mean curvature, convexity, geodesic depth, and travel depth for gray matter structure and fractional anisotropy, mean diffusivity, axial diffusivity, and radial diffusivity for white matter structure.

Figure 4

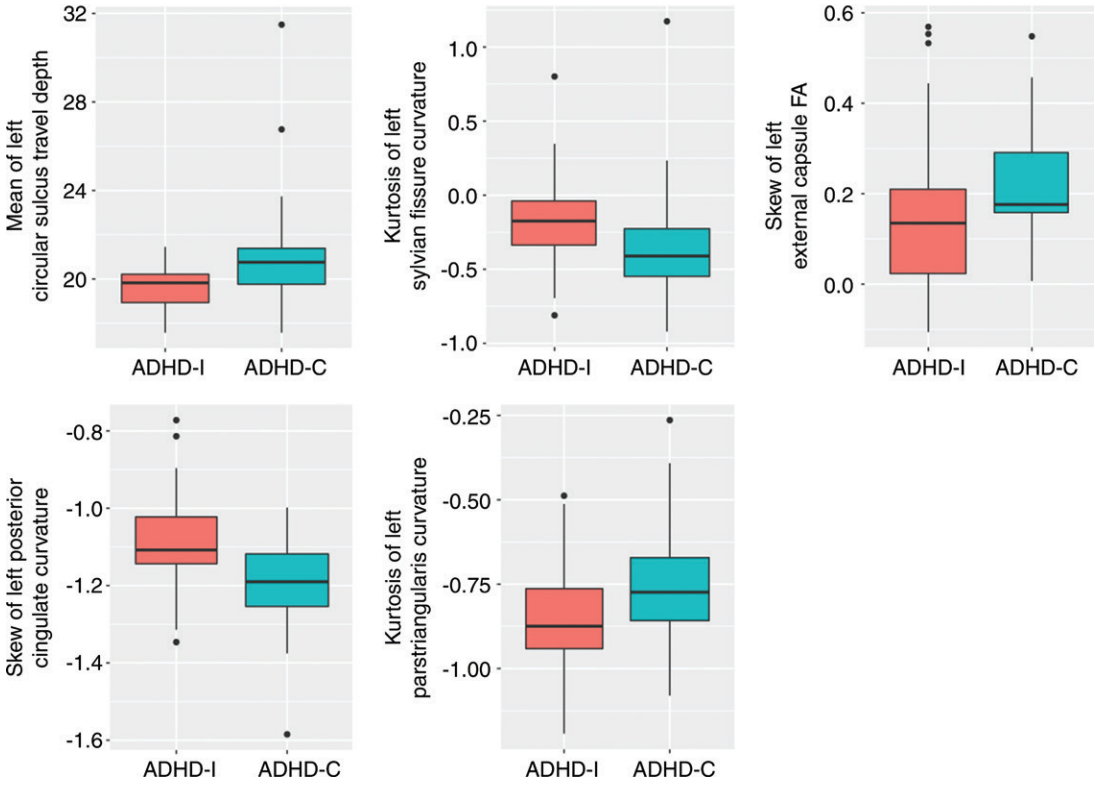

Figure 4: Distribution of significant features that discriminated ADHD-I and ADHD-C. *FA* = fractional anisotropy.

authors of many studies have reported white matter abnormalities in patients with ADHD.

In our study, we established an analysis framework on the basis of cerebral radiomics and machine learning methods for ADHD diagnosis and subtyping. Both structural and diffusion data were involved in the process of classifier building, providing a more comprehensive neuroanatomical evaluation of the disorder. By integrating the all-relevant features selection step, the random forest classifier allowed the achievement of average accuracy of 73.7% for identifying individuals with ADHD and 80.1% for discriminating between ADHD-I and ADHD-C, somewhat better than those achieved with the ADHD-200 consortium. In comparison with the commonly used minimal-optimal feature selection algorithm, the all-relevant features selection algorithm allows identification of all features

that provide information usable for classification, rather than finding a more compact subset of features on which a certain classifier has a minimal error. Thus, the proposed analytic framework has the ability to identify all features relevant to diagnosis and subtyping the two most common forms of ADHD and to advance a more comprehensive understanding of the neuroanatomic alterations related to ADHD and its most common subtypes.

In the human brain, the morphology of cortical gyri and sulci is complex and variable among individuals. This may cause and reflect abnormal functioning, with specific abnormalities observed in patients with developmental and neuropsychiatric disorders, but may also reflect the individual variation in neuroanatomy. Authors of previous ADHD research (34,35) suggest that aberrant cortical folding patterns may be involved in the pathology of ADHD. Local cortical thickness, convexity, curvature, and depth are frequently used shape analysis measures for characterizing cortical folding patterns. Results from the feature selection procedure in our study indicate that the top discriminative differences between patients with ADHD and typically developing control subjects are local alteration in cortical shape principally in the left temporal lobe, bilateral cuneus, and regions around the left central sulcus.

Structural changes in the motor area are of interest, because impaired motor inhibition is a cardinal feature of ADHD. Precentral and postcentral cortical areas also have been implicated in inhibitory behavioral control (36). By using shape measures, we found an altered distribution of the curvature of vertices within left precentral and postcentral regions. Curvature primarily reflects packing density and arrangement of neuronal cells (37). This result further refines conclusions from previous voxel-based morphometry studies in which authors reported reduced gray matter in the motor and premotor cortices (38), because alteration of gray matter volume identified with voxel-based morphometry can be sensitive to changes in gray matter and cerebral spinal fluid volumes as well as in cortical surface curvature (39). Findings of altered shape in the left temporal lobes are also, to some extent, consistent with previous morphometric studies in which authors observed a reduction in size of the anterior temporal lobes along with an increased density of gray matter in posterior temporal cortices. These temporal regions integrate information from lower-order sensory to higher-order perceptual systems used to guide the control of attention and action (40). Thus, observed abnormalities in the left temporal lobe may be clinically relevant with regard to cognitive and behavioral problems in patients with ADHD.

In comparison with prior findings of decreased total brain volume and global gray matter in children with ADHD (41), our study of never-treated patients showed no volume differences in total brain, white matter, or cortical and subcortical gray matter between patients with ADHD and control subjects. Differences in study methodologies and patient age and treatment history may have contributed to this discrepancy. Also, authors of previous studies reported cortical thinning in patients with ADHD, while we found increased cortical thickness throughout the bilateral cuneus in patients with ADHD relative to that in control subjects. The cuneus is central to processing visual information. This might underlie alterations in visual psychophysical processes related to visual sensation and perception in patients with ADHD (42). Results of a recent study showed that 11-year-old children with ADHD presented similar visual temporal selective attention as healthy 8-year-old control subjects (43), consistent with a neurodevelopmental delay affecting visual cortical systems. According to the typical trajectory of cortex maturation, cortical thickness declines in a relatively linear pattern after approximately 5 years of age (44). The observed thicker cuneus in patients with ADHD may thus suggest a developmental delay in the primary visual cortex in ADHD, but longitudinal developmental studies are needed to confirm this interpretation.

Different ADHD subtypes may share overlapping structural aberrations, but also exhibit unique abnormalities as suggested in prior work (45). However, authors of few studies to date have examined neuroanatomic differences between ADHD subtypes, to our knowledge. With the use of shape measurements, the feature selection process revealed differences between subtypes located in the circular sulcus, posterior cingulate cortex, sylvian fissure, and pars triangularis. These morphometric findings are consistent with a previous functional study, in which ADHD-C exhibited altered regional connectivity in the default mode network and insular cortex, while ADHD-I exhibited alteration in frontoparietal network (45). In addition, alterations in the posterior cingulate cortex, which is a key integration node in the default mode network, have been related to ADHD-I (46).

In comparison with widespread alterations in white matter revealed in previous studies in which group-level comparison was used, in our study, we identified local alterations in the skew of fractional anisotropic distribution linked to ADHD discrimination and subtyping. Decreased skew of fractional anisotropic distribution was found in the left cerebellar peduncle, a fiber bundle connecting the sensory and motor areas of the cortex with the pons and cerebellum. ADHD-I and ADHD-C also had differences in the skew of fractional anisotropic distribution in the left external capsule, which connects anterior and posterior attentional systems (47). Fractional anisotropy measurements in white matter have a very broad distribution with considerable skew and kurtosis (48), and the change in skew may reflect alterations of tissue organization. Because of the inherent limitation of the atlas used for parcellation, only main white matter tracts were evaluated in feature extraction. Future studies of fibers in superficial regions may provide additional information about the specific areas of cortex affected by tract alterations.

There were several limitations of this study that need to be taken into account when interpreting the data. First, because of the low prevalence of the hyperactive impulsive subtype of ADHD in China (49) and our restrictive inclusion criteria, individuals with this subtype were not included in our study. Second, children of a fairly large age range who were at different stages of their developmental trajectories participated in our study. This maturational heterogeneity may have limited the classification performance. Training and testing the classifier with samples from a narrower age range may allow better performance to be achieved, and the identified features and contribution to classification may shift with development. Last, whether patients with ADHD who were correctly classified with MR imaging represent a biologically homogeneous subgroup with distinct prognosis or treatment outcome remains to be investigated in future studies.

Our findings indicate that a moderately successful diagnostic classification efficiency can be achieved between patients with ADHD and healthy control subjects as well as between the two most common ADHD subtypes with the use of cerebral radiomic features. The workflow we used was automatic, and therefore, potentially useful clinically. In addition, our findings establish the potential utility of classification strategies with MR imaging data for diagnosis of a common mental disorder and provide new insights into the specific neurologic-anatomic features related to the disorder and its subtypes. Specifically, this study adds to the field of psychoradiology (*https://radiopaedia.org/articles/psychoradiology*), an evolving subspecialty of radiology, which is primed to be of major clinical importance in guiding diagnostic and therapeutic decision making in patients with mental disorders.

Disclosures of Conflicts of Interest: **H.S.** disclosed no relevant relationships. **Y.C.** disclosed no relevant relationships. **Q.H.** disclosed no relevant relationships. **S.L.** disclosed no relevant relationships. **X.H.** disclosed no relevant relationships. **Y.S.** disclosed no relevant relationships. **J.A.S.** Activities related to the present article: disclosed no relevant relationships. Activities not related to the present article: consultant for Takeda. Other relationships: disclosed no relevant relationships. **Q.G.** disclosed no relevant relationships.

References

1. American Psychiatric Association. Diagnostic and Statistical Manual of Mental Disorders. Physiol. Res. Arlington, Va: American Psychiatric Association, 2013.
2. Ek U, Westerlund J, Holmberg K, Fernell E. Academic performance of adolescents with ADHD and other behavioural and learning problems -a population-based longitudinal study. Acta Paediatr 2011;100(3):402–406.
3. Martel M, Nikolas M, Nigg JT. Executive function in adolescents with ADHD. J Am Acad Child Adolesc Psychiatry 2007;46(11):1437–1444.
4. Nijmeijer JS, Minderaa RB, Buitelaar JK, Mulligan A, Hartman CA, Hoekstra PJ. Attention-deficit/hyperactivity disorder and social dysfunctioning. Clin Psychol Rev 2008;28(4):692–708.
5. Shaw P, Stringaris A, Nigg J, Leibenluft E. Emotion dysregulation in attention deficit hyperactivity disorder. Am J Psychiatry 2014;171(3):276–293.
6. Willcutt EG. The prevalence of DSM-IV attention-deficit/hyperactivity disorder: a meta-analytic review. Neurotherapeutics 2012;9(3):490–499.
7. Colby JB, Rudie JD, Brown JA, Douglas PK, Cohen MS, Shehzad Z. Insights into multimodal imaging classification of ADHD. Front Syst Neurosci 2012;6:59.
8. Filipek PA, Semrud-Clikeman M, Steingard RJ, Renshaw PF, Kennedy DN, Biederman J. Volumetric MRI analysis comparing subjects having attention-deficit hyperactivity disorder with normal controls. Neurology 1997;48(3):589–601.
9. Castellanos FX, Lee PP, Sharp W, et al. Developmental trajectories of brain volume abnormalities in children and adolescents with attention-deficit/hyperactivity disorder. JAMA 2002;288(14):1740–1748.
10. Mostofsky SH, Cooper KL, Kates WR, Denckla MB, Kaufmann WE. Smaller prefrontal and premotor volumes in boys with attention-deficit/hyperactivity disorder. Biol Psychiatry 2002;52(8):785–794.
11. Valera EM, Faraone SV, Murray KE, Seidman LJ. Meta-analysis of structural imaging findings in attention-deficit/hyperactivity disorder. Biol Psychiatry 2007;61(12):1361–1369.
12. Nakao T, Radua J, Rubia K, Mataix-Cols D. Gray matter volume abnormalities in ADHD: voxel-based meta-analysis exploring the effects of age and stimulant medication. Am J Psychiatry 2011;168(11):1154–1163.
13. Ellison-Wright I, Ellison-Wright Z, Bullmore E. Structural brain change in Attention Deficit Hyperactivity Disorder identified by meta-analysis. BMC Psychiatry 2008;8(1):51.
14. Narr KL, Woods RP, Lin J, et al. Widespread cortical thinning is a robust anatomical marker for attention-deficit/hyperactivity disorder. J Am Acad Child Adolesc Psychiatry 2009;48(10):1014–1022.
15. van Ewijk H, Heslenfeld DJ, Zwiers MP, Buitelaar JK, Oosterlaan J. Diffusion tensor imaging in attention deficit/hyperactivity disorder: a systematic review and meta-analysis. Neurosci Biobehav Rev 2012;36(4):1093–1106.
16. Lemm S, Blankertz B, Dickhaus T, Müller KR. Introduction to machine learning for brain imaging. Neuroimage 2011;56(2):387–399.
17. Lui S, Zhou XJ, Sweeney JA, Gong Q. Psychoradiology: the frontier of neuroimaging in psychiatry. Radiology 2016;281(2):357–372.
18. Cox DD, Savoy RL. Functional magnetic resonance imaging (fMRI) "brain reading": detecting and classifying distributed patterns of fMRI activity in human visual cortex. Neuroimage 2003;19(2 Pt 1):261–270.
19. Ford J, Farid H, Makedon F, et al. Patient classification of fMRI activation maps. In: Ellis RE, Peters TM, eds. Medical Image Computing and Computer-Assisted Intervention - MICCAI 2003. MICCAI 2003. Lecture Notes in Computer Science, vol 2879. Berlin, Germany: Springer, 2003; 58–65.
20. Mourão-Miranda J, Bokde AL, Born C, Hampel H, Stetter M. Classifying brain states and determining the discriminating activation patterns: Support Vector Machine on functional MRI data. Neuroimage 2005;28(4):980–995.
21. Gillies RJ, Kinahan PE, Hricak H. Radiomics: images are more than pictures, they are data. Radiology 2016;278(2):563–577.
22. Lambin P, Rios-Velazquez E, Leijenaar R, et al. Radiomics: extracting more information from medical images using advanced feature analysis. Eur J Cancer 2012;48(4):441–446.
23. Chu C, Hsu AL, Chou KH, Bandettini P, Lin C; Alzheimer's Disease Neuroimaging Initiative.

Does feature selection improve classification accuracy? Impact of sample size and feature selection on classification using anatomical magnetic resonance images. Neuroimage 2012;60(1):59–70.

24. Chen ZJ, He Y, Rosa-Neto P, Germann J, Evans AC. Revealing modular architecture of human brain structural networks by using cortical thickness from MRI. Cereb Cortex 2008;18(10):2374–2381.
25. Spreng RN, Sepulcre J, Turner GR, Stevens WD, Schacter DL. Intrinsic architecture underlying the relations among the default, dorsal attention, and frontoparietal control networks of the human brain. J Cogn Neurosci 2013;25(1):74–86.
26. Klein A, Tourville J. 101 labeled brain images and a consistent human cortical labeling protocol. Front Neurosci 2012;6:171.
27. Tustison NJ, Cook PA, Klein A, et al. Large-scale evaluation of ANTs and FreeSurfer cortical thickness measurements. Neuroimage 2014;99:166–179.
28. Klein A, Ghosh SS, Bao FS, et al. Mindboggling morphometry of human brains. PLOS Comput Biol 2017;13(2):e1005350.
29. Kursa MB, Rudnicki WR. Feature selection with the Boruta package. J Stat Softw 2010;36(11):1–13.
30. Kim JH. Estimating classification error rate: Repeated cross-validation, repeated hold-out and bootstrap. Comput Stat Data Anal 2009;53(11):3735–3745.
31. Varma S, Simon R. Bias in error estimation when using cross-validation for model selection. BMC Bioinformatics 2006;7:91.
32. Wright SP. Adjusted P-values for simultaneous inference. Biometrics 1992;48(4):1005.
33. HD-200 Consortium. The ADHD-200 Consortium: a model to advance the translational potential of neuroimaging in clinical neuroscience. Front Syst Neurosci 2012;6:62.
34. Giedd JN, Rapoport JL. Structural MRI of pediatric brain development: what have we learned and where are we going? Neuron 2010;67(5):728–734.
35. Li X, Jiang J, Zhu W, et al. Asymmetry of prefrontal cortical convolution complexity in males with attention-deficit/hyperactivity disorder using fractal information dimension. Brain Dev 2007;29(10):649–655.
36. Luna B, Thulborn KR, Munoz DP, et al. Maturation of widely distributed brain function subserves cognitive development. Neuroimage 2001;13(5):786–793.
37. Selemon LD, Rajkowska G, Goldman-Rakic PS. Elevated neuronal density in prefrontal area 46 in brains from schizophrenic patients: application of a three-dimensional, stereologic counting method. J Comp Neurol 1998;392(3):402–412.
38. Carmona S, Vilarroya O, Bielsa A, et al. Global and regional gray matter reductions in ADHD: a voxel-based morphometric study. Neurosci Lett 2005;389(2):88–93.
39. Saute R, Dabbs K, Jones JE, Jackson DC, Seidenberg M, Hermann BP. Brain morphology in children with epilepsy and ADHD. PLoS One 2014;9(4):e95269.
40. Sowell ER, Thompson PM, Welcome SE, Henkenius AL, Toga AW, Peterson BS. Cortical abnormalities in children and adolescents with attention-deficit hyperactivity disorder. Lancet 2003;362(9397):1699–1707.
41. Shaw P, Eckstrand K, Sharp W, et al. Attention-deficit/hyperactivity disorder is characterized by a delay in cortical maturation. Proc Natl Acad Sci U S A 2007;104(49):19649–19654.
42. Peng X, Lin P, Zhang T, Wang J. Extreme learning machine-based classification of ADHD using brain structural MRI data. PLoS One 2013;8(11):e79476.
43. Donnadieu S, Berger C, Lallier M, Marendaz C, Laurent A. Is the impairment in temporal allocation of visual attention in children with ADHD related to a developmental delay or a structural cognitive deficit? Res Dev Disabil 2014;36C:384–395.
44. Ducharme S, Albaugh MD, Nguyen TV, et al. Trajectories of cortical thickness maturation in normal brain development--The importance of quality control procedures. Neuroimage 2016;125:267–279.
45. Fair DA, Nigg JT, Iyer S, et al. Distinct neural signatures detected for ADHD subtypes after controlling for micro-movements in resting state functional connectivity MRI data. Front Syst Neurosci 2013;6:80.
46. Anderson A, Douglas PK, Kerr WT, et al. Non-negative matrix factorization of multimodal MRI, fMRI and phenotypic data reveals differential changes in default mode subnetworks in ADHD. Neuroimage 2014;102 (Pt 1):207–219.
47. Pastura G, Doering T, Gasparetto EL, Mattos P, Araújo AP. Exploratory analysis of diffusion tensor imaging in children with attention deficit hyperactivity disorder: evidence of abnormal white matter structure. Atten Defic Hyperact Disord 2016;8(2):65–71.
48. Alexander AL, Lee JE, Lazar M, Field AS. Diffusion tensor imaging of the brain. Neurotherapeutics 2007;4(3):316–329.
49. Huang Y, Zheng S, Xu C, et al. Attention-deficit hyperactivity disorder in elementary school students in Shantou, China: prevalence, subtypes, and influencing factors. Neuropsychiatr Dis Treat 2017;13:785–792.